

Article

Ion Exchange of One-Pot Synthesized Cu-SAPO-44 with NH_4NO_3 to Promote Cu Dispersion and Activity for Selective Catalytic Reduction of NO_x with NH_3

Nana Zhang ¹, Ying Xin ^{1,*} , Qian Li ¹, Xicheng Ma ², Yongxin Qi ³, Lirong Zheng ⁴ and Zhaoliang Zhang ^{1,*}

¹ School of Chemistry and Chemical Engineering, Shandong Provincial Key Laboratory of Fluorine Chemistry and Chemical Materials, University of Jinan, Jinan 250022, China; chm_zhangnn@mail.ujn.edu.cn (N.Z.); chm_liqian@ujn.edu.cn (Q.L.)

² School of Chemistry and Chemical Engineering, Shandong University, Jinan 250100, China; maxch@sdu.edu.cn

³ School of Material Science and Technology, Shandong University, Jinan 250100, China; qyx66@sdu.edu.cn

⁴ Institute of High Energy Physics, Chinese Academy of Sciences, Beijing 100049, China; zhenglr@ihep.ac.cn

* Correspondence: chm_xiny@ujn.edu.cn (Y.X.); chm_zhangzl@ujn.edu.cn (Z.Z.); Tel.: +86-0531-8973-6032 (Y.X. & Z.Z.)

Received: 20 September 2019; Accepted: 22 October 2019; Published: 24 October 2019



Abstract: Cu-containing CHA type (Cu-CHA) zeolites have been widely investigated owing to their excellent low-temperature activity and high hydrothermal stability in selective catalytic reduction of NO_x with NH_3 (NH_3 -SCR). Herein, a series of Cu-SAPO-44 zeolites were prepared by one-pot method with dual-amine templates and the subsequent ion exchange (IE) with NH_4NO_3 . The effect of NH_4NO_3 treatment on Cu species was investigated by X-ray powder diffraction (XRD), N_2 adsorption-desorption isotherm, inductively coupled plasma (ICP); field-emission scanning electron microscope (FE-SEM), high-resolution transmission electron microscope (HRTEM), X-ray absorption fine structure (XAFS), and H_2 -temperature-programmed reduction (H_2 -TPR). The results indicated that—besides the main SAPO-44 structure—the CuO phase was detected by XRD in original samples. After IE with NH_4NO_3 , the Cu contents decreased greatly from ICP analysis. The removal of CuO agglomerations and the presence of highly dispersed CuO nanoparticles (~2.36 nm) were confirmed by SEM, TEM and H_2 -TPR. Furthermore, a significant increase in the proportion of isolated Cu^{2+} was derived from XAFS. As a result, the activity at higher temperature (≥ 350 °C) was improved a lot.

Keywords: selective catalytic reduction; nitrogen oxide; one-pot synthesis; Cu-SAPO-44; ion exchange; NH_4NO_3

1. Introduction

Aqueous ion exchange (IE) is the most widely used method in preparation of small pore Cu-chabazite (Cu-CHA) zeolites [1–3]. Multiple IE procedures are time consuming; therefore, one-pot synthesis methods were hence developed [4–9]. For instance, Ren et al. pioneered the synthesis of Cu-SSZ-13 using Cu^{2+} -tetraethylenepentamine (Cu-TEPA) complex as structure-directing agent (SDA), with Cu loading in the range 0–10 wt.% [10]. Soon after, Cu-SAPO-34 zeolites with controllable Cu-loadings were synthesized by one-pot method using Cu-TEPA and low-cost SDAs [6,11–13]. More recently, another Cu-CHA zeolite, Cu-SAPO-44, was also reported [14]. In contrast to IE method, one-pot method could directly introduce Cu^{2+} ions into zeolites frameworks, and thus achieve high Cu loading and high dispersion of Cu species, leading to excellent NH_3 -SCR activity [15].

The downside, however, is that one-pot synthesis method tend to introduce excessive Cu species into CHA zeolites, which is detrimental to the hydrothermal stability of Cu-CHA catalysts [5]. IE with NH_4NO_3 was discovered as an efficient approach to achieve moderate Cu-loadings in one-pot synthesis of Cu-CHA zeolites by removing the excessive Cu species [10,16,17]. Xie et al. reported that one-time IE with NH_4NO_3 was completely sufficient to eliminate excess Cu species from the SSZ-13 structure and re-disperse the remaining Cu^{2+} ions [15]. Guo et al. demonstrated that Cu^{2+} ions migrated from large cages to more stable locations in six-membered rings of CHA structure after IE with NH_4NO_3 [17]. Nevertheless, there still lacks direct observation on the structural change of Cu species from one-pot synthesized Cu-CHA zeolites.

Herein, a series of Cu-SAPO-44 zeolites were fabricated through one-pot method with the dual-amine templates (denoted as $\text{Cu}_x\text{-SAPO-44}$) followed with ion exchange with NH_4NO_3 solution (denoted as $\text{Cu}_x\text{-SAPO-44-IE}$). The effects of IE with NH_4NO_3 on the textural and physical-chemical properties of Cu-SAPO-44, as well as the nature and location of active Cu species, were investigated. Interestingly, IE with NH_4NO_3 removed excessive CuO agglomerations, leading to a high proportion of isolated Cu^{2+} ions responsible for the high SCR activity.

2. Results and Discussion

2.1. XRD

Figure 1 displays XRD patterns of Cu-SAPO-44 zeolites before and after IE with NH_4NO_3 . The diffraction peaks for all samples are in accordance with those of pure SAPO-44 reported in our previous work [18], confirming the CHA structure [14,19]. However, the CuO phase was present in $\text{Cu}_x\text{-SAPO-44}$. Interestingly, the $\text{Cu}_x\text{-SAPO-44-IE}$ samples show only diffraction patterns of SAPO-44, suggesting that IE with NH_4NO_3 can remove the excess CuO species and simultaneously retain the SAPO-44 structure.

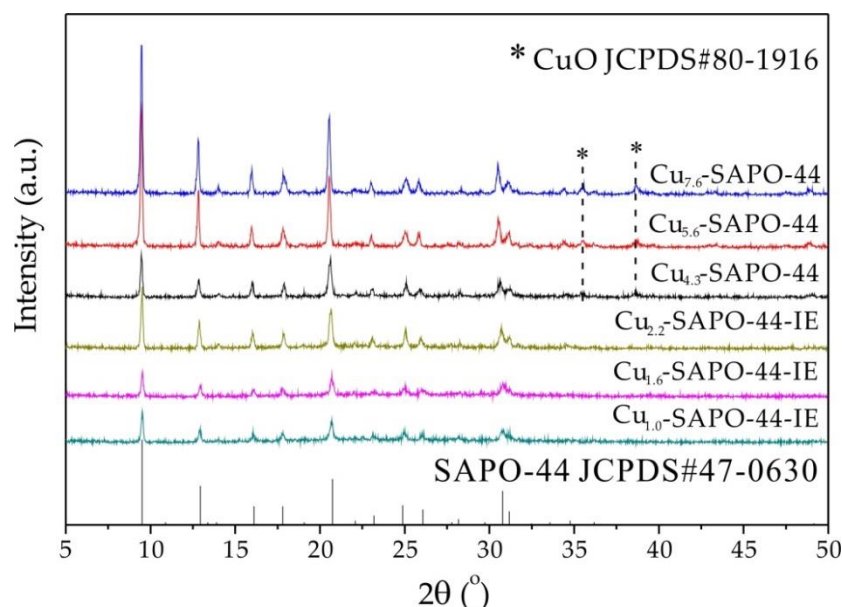


Figure 1. XRD patterns of $\text{Cu}_x\text{-SAPO-44}$ and $\text{Cu}_x\text{-SAPO-44-IE}$.

2.2. ICP

The compositions of all samples were analyzed by ICP and listed in Table 1. Although the Si/Al ratios do not change much after NH_4NO_3 treatment, the Cu contents decrease evidently after IE with NH_4NO_3 , in accordance with above XRD results.

Table 1. ICP results for Cu_x-SAPO-44 and Cu_x-SAPO-44-IE.

Sample	Element Content from ICP (wt.%)				
	Cu	Si	Al	Si/Al	P
Cu _{4.3} -SAPO-44	4.3	5.7	17.2	0.32	16.5
Cu _{5.6} -SAPO-44	5.6	6.4	16.7	0.37	13.6
Cu _{7.6} -SAPO-44	7.6	5.1	17.6	0.28	15.1
Cu _{1.0} -SAPO-44-IE	1.0	6.1	18.8	0.31	18.2
Cu _{1.6} -SAPO-44-IE	1.6	7.1	18.7	0.37	14.0
Cu _{2.2} -SAPO-44-IE	2.2	4.8	20.2	0.23	18.4

2.3. Catalytic Activity

SCR performances of Cu_x-SAPO-44 and Cu_x-SAPO-44-IE are shown in Figure 2. The Cu_x-SAPO-44 samples show 90% NO_x conversion between 200 and 350 °C as well as high N₂ selectivity. However, NO_x conversions decrease rapidly when the reaction temperatures are above 300 °C, due to the over-oxidation of NH₃ in the presence of CuO [15,20,21]. Notably, Cu_x-SAPO-44-IE samples exhibit improved NO_x conversion at high temperatures, reaching above 90% at 200–450 °C with nearly 100% N₂ selectivity. This is consistent with the fact that the excess CuO species promote the oxidation of NH₃ [10,15,17]. To gain more information about the beneficial role of IE, further characterization was performed taking the control sample (Cu_{5.6}-SAPO-44) and the best sample (Cu_{1.6}-SAPO-44-IE) as examples.

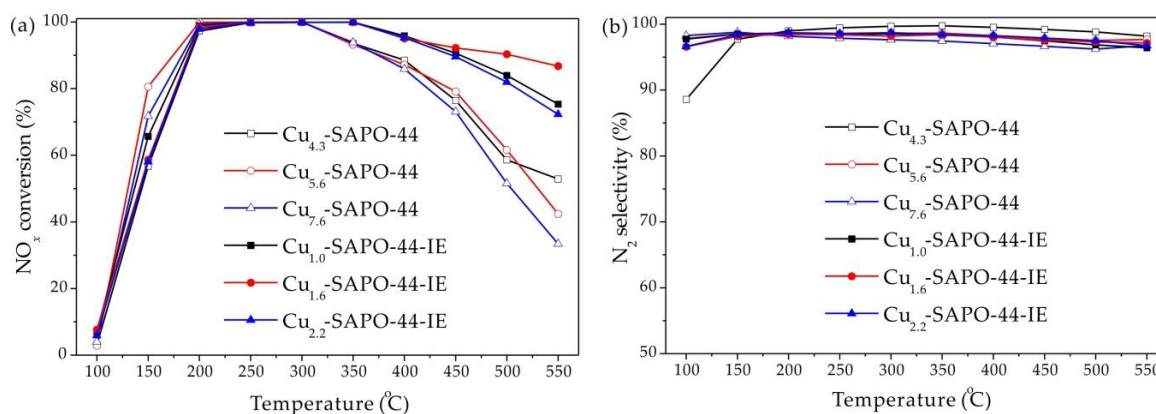


Figure 2. NO conversion (a) and N₂ selectivity (b) for Cu_x-SAPO-44 and Cu_x-SAPO-44-IE as a function of temperature. Reaction conditions: [O₂] = 5.3 vol.%, [NO] = [NH₃] = 500 ppm, balance He, total flow rate = 300 mL/min, GHSV = 100,000 h⁻¹.

Based on the practical consideration, NH₃-SCR performance of the Cu_{1.6}-SAPO-44-IE catalyst was also evaluated as 5 vol.% H₂O contained in feeding gas under the GHSV of 100,000 h⁻¹, and the result was shown in Figure 3. Unsurprisingly, a decrease in NO_x conversion was observed at low temperatures (<250 °C), which could be ascribed to the competitive adsorption of H₂O with NH₃. In contrast, NO_x conversion at high temperatures (>400 °C) was promoted, most likely due to the inhibition effect of H₂O on the unselective catalytic oxidation of NH₃ [22].

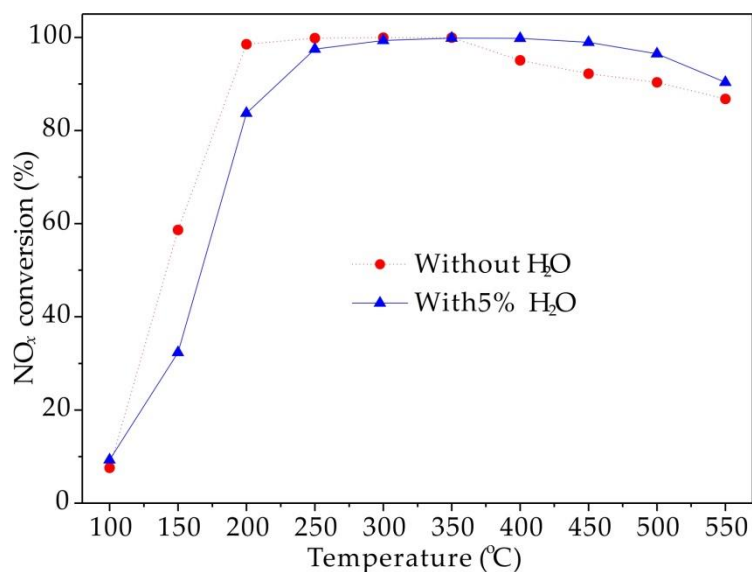


Figure 3. Effect of H₂O on NH₃-SCR performance of Cu_{1.6}-SAPO-44-IE.

2.4. N₂ Adsorption/Desorption

The N₂ adsorption/desorption isotherms of Cu_{5.6}-SAPO-44 and Cu_{1.6}-SAPO-44-IE exhibit the typical microporosity (Figure 4), similar to the pure SAPO-44 [18]. As a result, their BET surface areas are comparable. Furthermore, the pore volume of Cu_{1.6}-SAPO-44-IE slightly increased in comparison with Cu_{5.6}-SAPO-44 (Table 2), suggesting the CuO species that block the pores in CHA zeolite have been partially removed, as detected by ICP (Table 1).

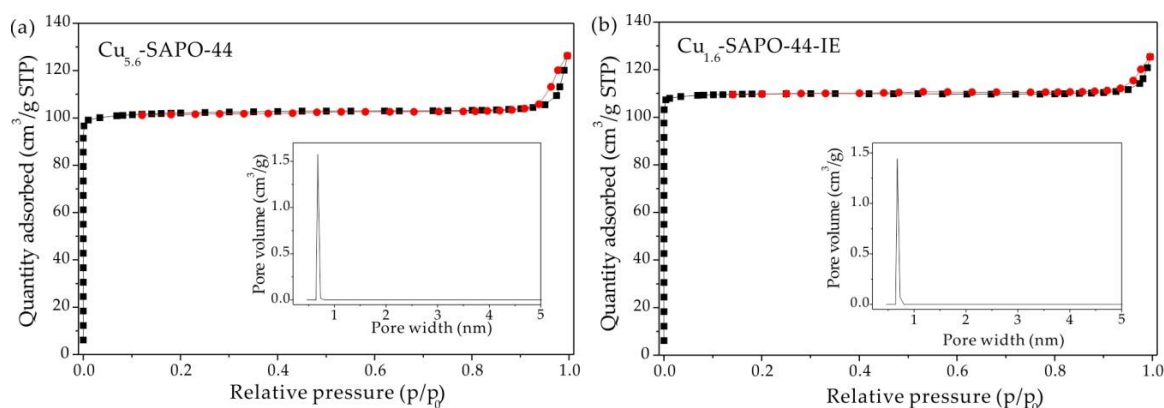


Figure 4. N₂ adsorption/desorption isotherms and pore diameter distribution for (a) Cu_{5.6}-SAPO-44 and (b) Cu_{1.6}-SAPO-44-IE.

Table 2. Textural properties and XAFS fitting results for Cu_{5.6}-SAPO-44 and Cu_{1.6}-SAPO-44-IE.

Sample	BET Surface Areas (m ² /g)	Pore Volume (cm ³ /g)	Cu ²⁺ /CuO Data from LCF of XANES Spectra (wt.%/wt.%)
Cu _{5.6} -SAPO-44	338.8	0.15	22.4/77.6
Cu _{1.6} -SAPO-44-IE	363.7	0.17	69.7/30.3

2.5. Electron Micrograph

SEM and TEM were conducted for Cu_{5.6}-SAPO-44 and Cu_{1.6}-SAPO-44-IE (Figure 5). It is notable that both Cu_{5.6}-SAPO-44 (Figure 5a,b) and Cu_{1.6}-SAPO-44-IE (Figure 5d,e) show the cubic-like rhombohedral morphology, similar to those reported in literature [19]. According to EDS elemental

mappings, some large Cu-containing agglomerations are observed in Cu_{5.6}-SAPO-44 that can be ascribed to the aggregated CuO nanoparticles (Figure 5c), owing to its high Cu content. As reported by He et al., the excess Cu species in Cu-SSZ-13 zeolites could be effectively removed by ion exchange using NH₄NO₃ solution [15]. Accordingly, large CuO particles can be scoured into CuO nanocrystals and re-dispersed as Cu²⁺ ions during this ion exchange process. In this work, after IE with NH₄NO₃, highly dispersed Cu-containing species were observed over the entire zeolite as for Cu_{1.6}-SAPO-44-IE (Figure 5f), which can be attributed to the remaining CuO nanoparticles and Cu²⁺ ions at the framework ion-exchange sites. In order to clarify the highly dispersed Cu-containing species after IE with NH₄NO₃, Cu_{1.6}-SAPO-44-IE was further characterized by TEM (Figure 5g–i). The well-dispersed nanocrystals were observed in Cu_{1.6}-SAPO-44-IE (Figure 5g), which were proved to be CuO nanoparticles by identifying the characteristic spacings of 2.27 and 1.87 Å for the (2 0 0) and the (-2 0 2) lattice planes of monoclinic CuO (Figure 5h). A particle count taken from many TEM images, obtained from different regions of the sample, confirmed the presence of monodispersed CuO nanoparticles with a mean diameter of 2.36 nm anchored on the surface of Cu_{1.6}-SAPO-44-IE (Figure 5i). Combined with ICP data, the results confirm that IE with NH₄NO₃ can not only remove the excessive Cu species (in the form of CuO agglomerations) but also improve the dispersion of the remaining CuO nanoparticles. This result is consistent with the observation from other researchers that CuO aggregates decrease the SCR performance at high temperature range as a result of parasitic NH₃ oxidation [15,23].

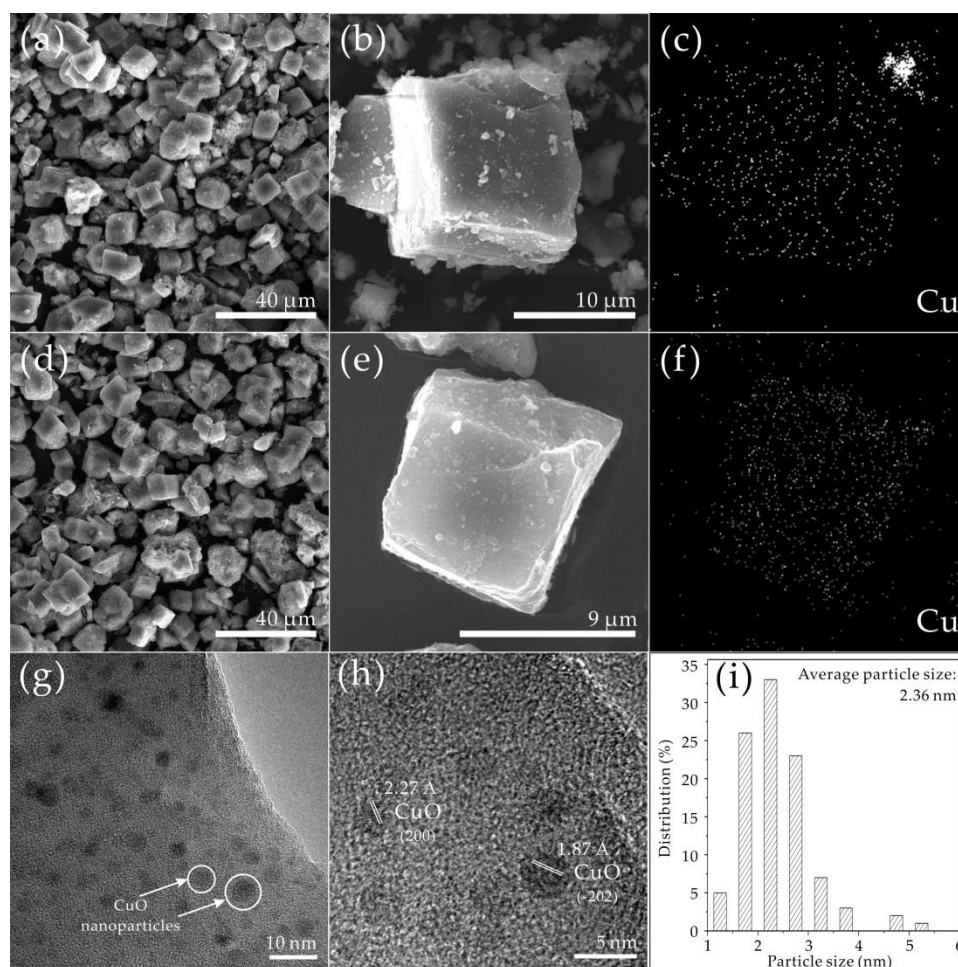


Figure 5. Electron micrograph of Cu_{5.6}-SAPO-44 and Cu_{1.6}-SAPO-44-IE. FESEM images for Cu_{5.6}-SAPO-44 (a,b) and Cu_{1.6}-SAPO-44-IE (d,e), Cu mapping for Cu_{5.6}-SAPO-44 (c) and Cu_{1.6}-SAPO-44-IE (f); TEM image (g), HRTEM image (h) and particle size distribution of CuO nanoparticles (i) of Cu_{1.6}-SAPO-44-IE.

2.6. H₂-TPR

H₂-TPR was also performed on Cu_{5.6}-SAPO-44 and Cu_{1.6}-SAPO-44-IE, and the results were shown in Figure 6. For Cu_{5.6}-SAPO-44 (a), the obvious reduction peak centered at ~300 °C could be ascribed to the reduction of CuO (>3 nm) to Cu⁰ [24]. However, this peak disappeared in Cu_{1.6}-SAPO-44-IE (b), and a broad reduction peak ranging from 160 to 750 °C emerged, suggesting the removal of large agglomerated CuO particles and the existence of highly dispersed Cu²⁺ and CuO microcrystals after NH₄NO₃ treatment, in accordance with the results of XRD and SEM.

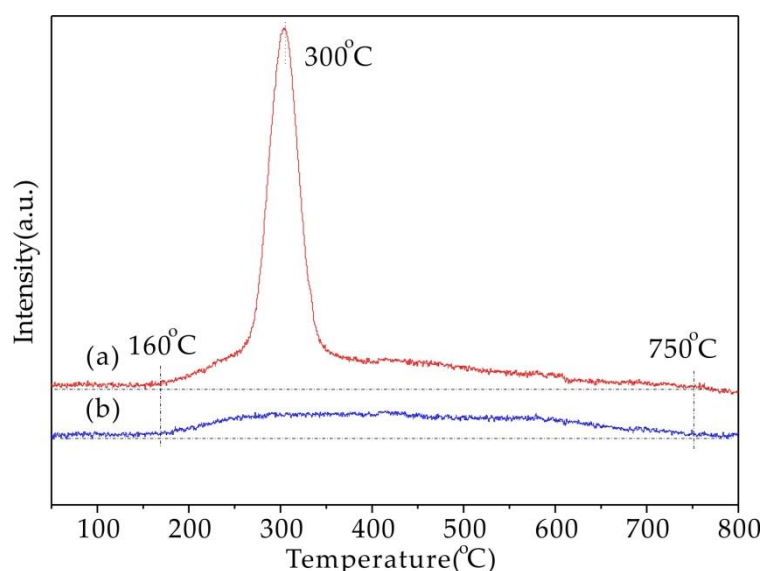


Figure 6. H₂-TPR profiles of Cu_{5.6}-SAPO-44 (a) and Cu_{1.6}-SAPO-44-IE (b).

2.7. XAFS

Individual Cu species were studied by XAFS in combination with linear combination fitting. Figure 7a shows the X-ray absorption near edge structure (XANES) spectra of Cu K-edge for Cu_{5.6}-SAPO-44, Cu_{1.6}-SAPO-44-IE, and reference samples. The XANES spectrum of Cu_{5.6}-SAPO-44 resembled that of CuO, while that for Cu_{1.6}-SAPO-44-IE is similar to that of CuSO₄. The corresponding Fourier-transformed k³-weighted Cu K-edge patterns give more direct evidence (Figure 7b). In the case of Cu_{5.6}-SAPO-44, two characteristic peaks at approximately 2.6 and 3.0 Å were detected, which are attributed to the neighboring Cu atoms (Cu-O-Cu) in CuO [25]. For Cu_{1.6}-SAPO-44-IE, the peak at ~1.5 Å assigned to the Cu-O scatterings is similar with that of CuSO₄, confirming the predominance of isolated mononuclear Cu²⁺ species [26]. In addition, weak peaks at ~2.5 Å for Cu_{1.6}-SAPO-44-IE were distinguished, indicating the coexistence of few CuO nanoparticles. The relative amount of Cu²⁺ and CuO could be obtained from the intense analysis of XANES spectra using linear combination fitting (LCF) [27]. For Cu_{5.6}-SAPO-44, the majority of Cu species are CuO nanoparticles, while the Cu²⁺ ions are dominant in Cu_{1.6}-SAPO-44-IE (Figure 8). Thus, the isolated Cu²⁺ proportion was significantly improved via IE.

Consequently, the enhanced high-temperatures activity is attributed to the removal of CuO agglomerations and the relocation of the Cu²⁺ ions for Cu_x-SAPO-44-IE [10,17]. However, Cu_{1.6}-SAPO-44-IE still exhibited lower activity at high temperature (350–550 °C) compared with the traditional ion-exchanged counterpart with a comparative Cu content that contains only isolated Cu²⁺ ions [28].

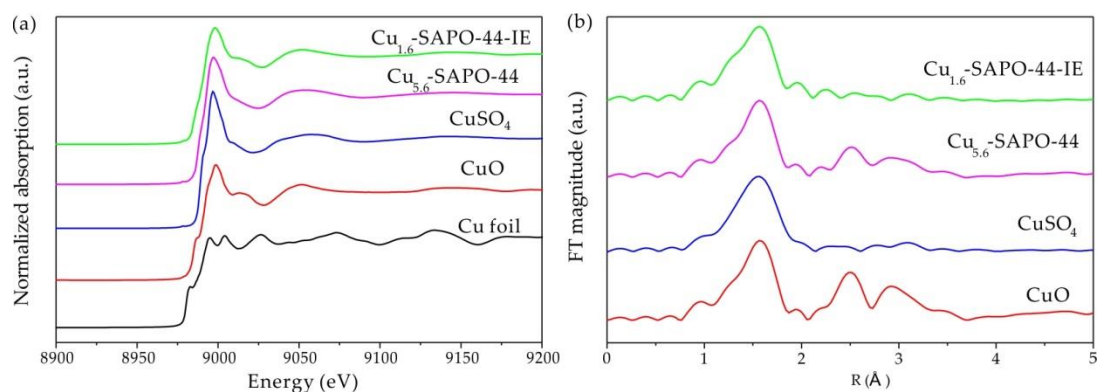


Figure 7. XANES (a), and FT-EXAFS (b) of Cu K-edge spectra for $\text{Cu}_{5.6}$ -SAPO-44, $\text{Cu}_{1.6}$ -SAPO-44-IE and the references.

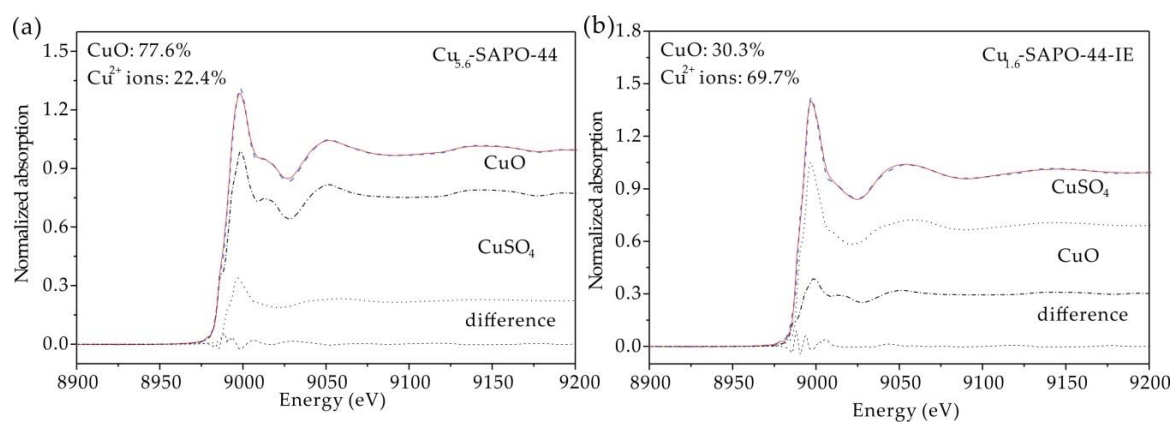


Figure 8. Linear combination fitting (LCF) of XANES spectra for (a) $\text{Cu}_{5.6}$ -SAPO-44, (b) $\text{Cu}_{1.6}$ -SAPO-44-IE.

3. Materials and Methods

3.1. Catalyst Preparation

In preparation of Cu-SAPO-44, the gel has a molar ratio of 0.14–0.22 Cu:0.44 TEPA:0.6 SiO_2 :0.8 Al_2O_3 :1 P_2O_5 :40 H_2O :2 N,N,N',N'-tetramethyl-1,6-hexanediamine (TMHD). CuSO_4 solution (20 wt.%) and TEPA were mixed under vigorous stirring at room temperature to get a homogeneous sol. After that, phosphoric acid (H_3PO_4 , 85 wt.% aqueous solution), pseudo-boehmite (Al_2O_3 , 78 wt.%), colloidal silica sol (30 wt.% suspension in water), TMHD template and deionized water were added to the Cu-TEPA complex solution under vigorous stirring. Then, the resulting viscous gel was aged with stirring at room temperature over 12 h, and further hydrothermally heated statically in a Teflon-lined steel autoclave at 200 °C for 96 h. The product was obtained by centrifugal, washed several times with deionized water, and dried at 100 °C for 12 h. Cu_x -SAPO-44 zeolites were obtained by calcination at 550 °C for 6 h in air to remove the structure-directing agent, where “x” represents the Cu content in the catalyst determined by ICP analysis.

In this study, the as-prepared Cu-CHA zeolite samples, have high Cu contents of 4.3, 5.6, and 7.6 wt.% respectively. Then unroasted Cu_x -SAPO-44 (1 g) zeolites were conducted ion exchange with 1.0 M NH_4NO_3 solution at 80 °C for 8 h to remove the abundant Cu, and dried Cu_x -SAPO-44-IE (0.9 g) can be obtained. Finally, the dried samples were calcined at 550 °C for 6 h [17] to remove structure-directing agent, and obtained Cu_x -SAPO-44-IE, samples with Cu contents of 1.0, 1.6, and 2.2 wt.% (corresponding original $x = 4.3, 5.6,$ and 7.6 wt.%, respectively).

3.2. Catalyst Characterizations

X-ray diffraction (XRD) was used to obtain the information about the crystalline structure of the catalysts, and equipped with Cu K α radiation ($\lambda = 1.5418 \text{ \AA}$). The BET surface area and pore size distribution of Cu_{5.6}-SAPO-44 and Cu_{1.6}-SAPO-44-IE were determined using BET measurements (Micromeritics ASAP 2020, Norcross, GA, USA) after dehydration of the catalysts at 300 °C for 9 h under vacuum. ICP-atomic emission spectrometry (ICP-AES) was carried out to determine the elemental contents of samples by using a PerkinElmer Optima 2100DV (Waltham, MA, USA). FE-SEM equipped with energy dispersive spectroscopy (EDS) was performed on a Hitachi SU-70 microscope (Tokyo, Japan). HRTEM was conducted on a JEOL JEM-2010 (Tokyo, Japan) and a FEI Tecnai G2 F20 transmission electron microscope operating at 200 kV. H₂-TPR experiments were performed on a chemisorption analyzer (XianQuan, TP-5000, TianJin, China). The samples (50 mg) were pretreated with pure O₂ flow at 500 °C for 30 min, and cooled down to the room temperature in the presence of O₂. Subsequently, the samples were reduced under a flow of 5 vol.% H₂/N₂ (50 mL/min) and then was heated to 800 °C with the rate of 10 °C/min. XAFS spectra were measured for the Cu K-edge at 1W1B beamline of Beijing synchrotron radiation facility (BSRF, Beijing, China) in the transmission mode and fluorescence mode at room temperature. XAFS raw data were analyzed using IFEFFIT software package [29].

3.3. Catalyst Activity Measurements

The steady state NH₃-SCR activity tests of Cu-SAPO-44 catalysts (~120 mg, 40–60 meshes) were performed at atmospheric pressure in a fixed-bed quartz tube reactor (6.0 mm i.d.). The gas consisting of 500 ppm NO, 500 ppm NH₃, 5.3 vol. % O₂, 5 vol. % H₂O (when used) and balance, He. The total gas flow rate was 300 mL/min, corresponding to a gas hourly space velocity (GHSV) of 100,000 h⁻¹. The measurement was carried out in the temperature range 100–550 °C. The NO and NO₂ concentrations of the reactor inlet/outlet were monitored by a chemiluminescence NO_x analyzer (42i-HL, Thermo, Waltham, MA, USA). In addition, N₂O and NH₃ were detected by quadrupole mass spectrometer (MS, OmniStar 200, Balzers, Switzerland) with a m/z of 44 for N₂O, and 17 for NH₃. During the test, each temperature point is stable for at least 30 min. The catalytic activity and N₂ selectivity were calculated according to the following equations:

$$\text{NO}_x \text{ conversion (\%)} = \frac{[\text{NO}_x]_{\text{in}} - [\text{NO}_x]_{\text{out}}}{[\text{NO}_x]_{\text{in}}} \times 100\%$$

$$\text{N}_2 \text{ selectivity (\%)} = \frac{[\text{NO}_x]_{\text{in}} + [\text{NH}_3]_{\text{in}} - [\text{NO}_x]_{\text{out}} - [\text{NH}_3]_{\text{out}} - 2[\text{N}_2\text{O}]}{[\text{NO}_x]_{\text{in}} + [\text{NH}_3]_{\text{in}} - [\text{NO}_x]_{\text{out}} - [\text{NH}_3]_{\text{out}}} \times 100\%$$

4. Conclusions

Cu-SAPO-44 zeolites were synthesized using a one-pot approach with dual-amine templates. Furthermore—although the total content of Cu was decreased—the CuO dispersion and isolated Cu²⁺ proportion were significantly improved via the subsequent IE with NH₄NO₃. The SCR activity was thus promoted at higher temperature. Cu_{1.6}-SAPO-44-IE shows >90% NO_x conversion in the temperature range 200–500 °C.

Author Contributions: Conceptualization, N.Z., Y.X. and Z.Z.; data curation, N.Z. and Y.X.; formal analysis, N.Z., Y.X., Q.L., and Z.Z.; funding acquisition, Y.X. and Z.Z.; investigation, N.Z., X.M., Y.Q., L.Z. and Y.X.; methodology, N.Z., L.Z. and Y.X.; writing—original draft, N.Z. and Y.X.; writing—review and editing, Z.Z.

Funding: This research was funded by National Natural Science Foundation of China (Grant No. 21906063 and 21876061) and Key Technology R&D Program of Shandong Province (Grant No. 2019GSF109042).

Conflicts of Interest: The authors declare no conflict of interest.

References

1. Kwak, J.H.; Tonkyn, R.G.; Kim, D.H.; Szanyi, J.; Peden, C.H.F. Excellent activity and selectivity of Cu-SSZ-13 in the selective catalytic reduction of NO_x with NH₃. *J. Catal.* **2010**, *275*, 187–190. [[CrossRef](#)]
2. Gao, F.; Walter, E.D.; Washton, N.M.; Szanyi, J.; Peden, C.H.F. Synthesis and evaluation of Cu-SAPO-34 catalysts for ammonia selective catalytic reduction. 1. Aqueous solution ion exchange. *ACS Catal.* **2013**, *3*, 2083–2093. [[CrossRef](#)]
3. Fickel, D.W.; D'Addio, E.; Lauterbach, J.A.; Lobo, R.F. The ammonia selective catalytic reduction activity of copper-exchanged small-pore zeolites. *Appl. Catal. B Environ.* **2011**, *102*, 441–448. [[CrossRef](#)]
4. Wang, J.H.; Zhao, H.W.; Haller, G.; Li, Y.D. Recent advances in the selective catalytic reduction of NO_x with NH₃ on Cu-chabazite catalysts. *Appl. Catal. B Environ.* **2017**, *202*, 346–354. [[CrossRef](#)]
5. Beale, A.M.; Gao, F.; Lezcano-Gonzalez, I.; Peden, C.H.F.; Szanyi, J. Recent advances in automotive catalysis for NO_x emission control by small-pore microporous materials. *Chem. Soc. Rev.* **2015**, *44*, 7371–7405. [[CrossRef](#)] [[PubMed](#)]
6. Turrina, A.; Eschenroeder, E.C.V.; Bode, B.E.; Collier, J.E.; Apperley, D.C.; Cox, P.A.; Casci, J.L.; Wright, P.A. Understanding the structure directing action of copper-polyamine complexes in the direct synthesis of Cu-SAPO-34 and Cu-SAPO-18 catalysts for the selective catalytic reduction of NO with NH₃. *Microporous Mesoporous Mater.* **2015**, *215*, 154–167. [[CrossRef](#)]
7. Xin, Y.; Li, Q.; Zhang, Z.L. Zeolitic materials for deNO_x selective catalytic reduction. *ChemCatChem* **2018**, *10*, 29–41. [[CrossRef](#)]
8. Shan, W.P.; Song, H. Catalysts for the selective catalytic reduction of NO_x with NH₃ at low temperature. *Catal. Sci. Technol.* **2015**, *5*, 4280–4288. [[CrossRef](#)]
9. Liu, F.D.; Yu, Y.B.; He, H. Environmentally-benign catalysts for the selective catalytic reduction of NO_x from diesel engines: Structure-activity relationship and reaction mechanism aspects. *Chem. Commun.* **2014**, *50*, 8445–8463. [[CrossRef](#)]
10. Ren, L.M.; Zhu, L.F.; Yang, C.G.; Chen, Y.M.; Sun, Q.; Zhang, H.Y.; Li, C.J.; Nawaz, F.; Meng, X.J.; Xiao, F.S. Designed copper-amine complex as an efficient template for one-pot synthesis of Cu-SSZ-13 zeolite with excellent activity for selective catalytic reduction of NO_x by NH₃. *Chem. Commun.* **2011**, *47*, 9789–9791. [[CrossRef](#)]
11. Martínez-Franco, R.; Moliner, M.; Franch, C.; Kustov, A.; Corma, A. Rational direct synthesis methodology of very active and hydrothermally stable Cu-SAPO-34 molecular sieves for the SCR of NO_x. *Appl. Catal. B Environ.* **2012**, *127*, 273–280. [[CrossRef](#)]
12. Deka, U.; Lezcano-Gonzalez, I.; Warrender, S.J.; Picone, A.L.; Wright, P.A.; Weckhuysen, B.M.; Beale, A.M. Changing active sites in Cu-CHA catalysts: deNO_x selectivity as a function of the preparation method. *Microporous Mesoporous Mater.* **2013**, *166*, 144–152. [[CrossRef](#)]
13. Gao, F.; Walter, E.D.; Washton, N.M.; Szanyi, J.; Peden, C.H.F. Synthesis and evaluation of Cu-SAPO-34 catalysts for NH₃-SCR 2: Solid-state ion exchange and one-pot synthesis. *Appl. Catal. B Environ.* **2015**, *162*, 501–514. [[CrossRef](#)]
14. Xin, Y.; Zhang, N.N.; Wang, X.; Li, Q.; Ma, X.C.; Qi, Y.X.; Zheng, L.R.; Anderson, J.A.; Zhang, Z.L. Efficient synthesis of the Cu-SAPO-44 zeolite with excellent activity for selective catalytic reduction of NO_x by NH₃. *Catal. Today* **2019**, *332*, 35–41. [[CrossRef](#)]
15. Xie, L.J.; Liu, F.D.; Ren, L.M.; Shi, X.L.; Xiao, F.S.; He, H. Excellent performance of one-pot synthesized Cu-SSZ-13 catalyst for the selective catalytic reduction of NO_x with NH₃. *Environ. Sci. Technol.* **2014**, *48*, 566–572. [[CrossRef](#)] [[PubMed](#)]
16. Ren, L.M.; Zhang, Y.B.; Zeng, S.J.; Zhu, L.F.; Sun, Q.; Zhang, H.Y.; Yang, C.G.; Meng, X.J.; Yang, X.G.; Xiao, F.S. Design and synthesis of a catalytically active Cu-SSZ-13 zeolite from a copper-amine complex template. *Chin. J. Catal.* **2012**, *33*, 92–105. [[CrossRef](#)]
17. Guo, Q.; Fan, F.; Ligthart, D.A.J.M.; Li, G.; Feng, Z.; Hensen, E.J.M.; Li, C. Effect of the nature and location of copper species on the catalytic nitric oxide selective catalytic reduction performance of the copper/SSZ-13 zeolite. *ChemCatChem* **2014**, *6*, 634–639. [[CrossRef](#)]
18. Li, H.; Xin, Y.; Wang, X.; Zhou, Y.H.; Li, Q.; Zhang, Z.L. A novel dual-template method for synthesis of SAPO-44 zeolite. *RSC Adv.* **2016**, *6*, 35910–35913. [[CrossRef](#)]

19. Xin, Y.; Wang, X.; Li, Q.; Ma, X.C.; Qi, Y.X.; Zheng, L.R.; Anderson, J.A.; Zhang, Z.L. The potential of Cu-SAPO-44 in selective catalytic reduction of NO_x with NH₃. *ChemCatChem* **2016**, *8*, 3740–3745. [[CrossRef](#)]
20. Xue, J.J.; Wang, X.Q.; Qi, G.; Wang, J.; Shen, M.Q.; Li, W. Characterization of copper species over Cu/SAPO-34 in selective catalytic reduction of NO_x with ammonia: Relationships between active Cu sites and de-NO_x performance at low temperature. *J. Catal.* **2013**, *297*, 56–64. [[CrossRef](#)]
21. Wang, L.; Li, W.; Qi, G.; Weng, D. Location and nature of Cu species in Cu/SAPO-34 for selective catalytic reduction of NO with NH₃. *J. Catal.* **2012**, *289*, 21–29. [[CrossRef](#)]
22. Li, J.; Chang, H.; Ma, L.; Hao, J.; Yang, R.T. Low-temperature selective catalytic reduction of NO_x with NH₃ over metal oxide and zeolite catalysts-A review. *Catal. Today* **2011**, *175*, 147–156. [[CrossRef](#)]
23. Gao, F.; Walter, E.D.; Karp, E.M.; Luo, J.; Tonkyn, R.G.; Kwak, J.H.; Szanyi, J.; Peden, C.H.F. Structure-activity relationships in NH₃-SCR over Cu-SSZ-13 as probed by reaction kinetics and EPR studies. *J. Catal.* **2013**, *300*, 20–29. [[CrossRef](#)]
24. Richter, M.; Fait, M.J.G.; Eckelt, R.; Schneider, M.; Radnik, J.; Heidemann, D.; Fricke, R. Gas-phase carbonylation of methanol to dimethyl carbonate on chloride-free Cu-precipitated zeolite Y at normal pressure. *J. Catal.* **2007**, *245*, 11–24. [[CrossRef](#)]
25. Yamashita, H.; Matsuoka, M.; Tsuji, K.; Shioya, Y.; Anpo, M.; Che, M. In-situ XAFS, photoluminescence, and IR investigations of copper ions included within various kinds of zeolites. Structure of Cu(I) ions and their interaction with CO molecules. *J. Phys. Chem.* **1996**, *100*, 397–402. [[CrossRef](#)]
26. Korhonen, S.T.; Fickel, D.W.; Lobo, R.F.; Weckhuysen, B.M.; Beale, A.M. Isolated Cu²⁺ ions: Active sites for selective catalytic reduction of NO. *Chem. Commun.* **2011**, *47*, 800–802. [[CrossRef](#)] [[PubMed](#)]
27. Gaur, A.; Shrivastava, B.D.; Joshi, S.K. Copper K-edge XANES of Cu(I) and Cu(II) oxide mixtures. *J. Phys. Conf. Ser.* **2009**, *190*, 012084. [[CrossRef](#)]
28. Peng, Z.L. *The Optimization on in Situ Synthesis Conditions of Cu-SSZ-13 Denitration Catalyst*; Taiyuan University of Technology: Taiyuan, China, 2015.
29. Newville, M. IFEFFIT: Interactive XAFS analysis and FEFF fitting. *J. Synchrotron Radiat.* **2001**, *8*, 322–324. [[CrossRef](#)]

